ELSEVIER

International Journal of Heat and Fluid Flow 22 (2001) 143–155

International Journal of HEAT AND FLUID FLOW

www.elsevier.com/locate/ijhff

Predictions of effect of swirl on flow and heat transfer in a rotating cavity

Hasan Karabay, Michael Wilson, J. Michael Owen *

Department of Mechanical Engineering, University of Bath, Bath BA2 7AY, UK

Received 16 October 1999; accepted 2 October 2000

Abstract

Pre-swirl nozzles are used to deliver the cooling air to the rotating turbine blades in the cooling systems of gas turbine engines. This paper considers the case where the cooling air flows radially outward, between two corotating discs, to create a free vortex in the inviscid core between the boundary layers on the discs. A thermodynamic analysis is used to relate the temperature increase of the cooling air to the adiabatic work term (which reduces the air temperature) and to the heat transfer from the discs to the air (which increases the temperature). The Reynolds analogy has been used to determine an expression for the adiabatic-disc temperature and to draw conclusions about the moment coefficient and average Nusselt number. An important parameter is β_p, the ratio of the tangential velocity of the pre-swirl air to the speed of the rotating disc, and the Reynolds analogy shows that the moment coefficient is zero when $\beta_p = \beta_{p,crit}$, a critical pre-swirl ratio, and that the average Nusselt number is a minimum when $\beta_p = \beta_{p,opt}$, an optimal pre-swirl ratio. Computations made using a steady-state axisymmetric elliptic-flow solver, incorporating a low-Reynolds-number k–ϵ turbulence model, are in good agreement with the pressure distribution, adiabatic-disc temperature and local Nusselt numbers predicted by the theoretical models. The computed values of $\beta_{p,crit}$ agree with the theoretical values, and the computations also confirm the occurrence of a minimum average Nusselt number. For $\beta_p < \beta_{p,opt}$, the computed temperature of the cooling air decreases as β_p increases; for $\beta_p > \beta_{p,opt}$, whether the temperature decreases or increases depends on the relative magnitude of the adiabatic work term and the heat transfer from the discs.

1. Introduction

In many gas turbines, the blade-cooling air is supplied from stationary pre-swirl nozzles, and a simplified diagram of the so-called "cover-plate pre-swirl system" is shown in Fig. 1. By swirling the air in the direction of rotation of the turbine disc, the relative temperature of the air entering the blade-cooling passages is reduced. Pre-swirl systems have been studied by a number of research workers, and the reader is referred to the work of Meierhofer and Franklin (1981), El-Oun and Owen (1989), Chen et al. (1993a,b), Popp et al. (1996), Wilson et al. (1997), Pilbrow et al. (1999) and Karabay et al. (1999, 2000). More general cases of rotating-disc flows can be found in Owen and Rogers (1989, 1995).

The work described below uses the so-called "simple rotating cavity" between the rotating disc and the cover-plate as a simplified model of the complete pre-swirl cover-plate system. The aims of the paper are to provide a theoretical framework for pre-swirl systems and to show the effects of the flow parameters on the velocity, pressure and Nusselt numbers in the rotating cavity. Whilst the complete system is more complex, the simple cavity provides insight into this complicated problem.

The axisymmetric computational model is described in Section 2, and Sections 3 and 4 deal, respectively, with the fluids dynamics and thermodynamics of the problem. In Section 5, the Reynolds analogy is used to determine the effect of swirl on the adiabatic-disc temperature and on the local and average Nusselt numbers for the simple cavity. The Reynolds analogy is also used in Section 6, where the effect of the pre-swirl ratio on the moment coefficients and the heat transfer is examined; in particular, a critical pre-swirl ratio, at which the moment coefficient is zero, and an optimal pre-swirl, at which the average Nusselt number is a minimum, are discussed. Conclusions are presented in Section 7.

2. Computational model

The geometry of the simple rotating cavity and the computational grid used in this study are shown in Fig. 2, and the dimensions are: $a = r_p = r_1 = 100$ mm, $r_b = r_2 = 200$ mm, $b = 206$ mm, $\Delta r_b = 2.2$ mm, $s = 10$ mm ($G = s/b = 0.0485$, $a/b = 0.485$, $x_1/x_2 = 0.5$).

The ranges of flow parameters used in the computations were: $0.1 < \lambda_T < 0.4$, $0.6 \times 10^6 < Re_\phi < 1.8 \times 10^6$, $5800 < C_w < 23000$, $0 < \beta_p < 6$. The values of λ_T and β_p determine the

* Corresponding author. Tel.: +44-1225-826-934; fax: +44-1225-82-6928.

E-mail address: j.m.owen@bath.ac.uk (J.M. Owen).

0142-727X/01/$ - see front matter
PII: S0142-727X(00)00076-X

Notation

a	inner radius of cavity
b	outer radius of cavity
C_m	moment coefficient
C_p	pressure coefficient
c_p, c_v	specific heat at constant pressure and constant volume, respectively
C_w	nondimensional mass flow rate ($= \dot{m}/\mu b$)
H	total enthalpy ($= c_pT + (1/2)(V_r^2 + V_\phi^2 + V_z^2) + k'p/\rho$)
G	gap ratio ($= s/b$)
k	turbulent kinetic energy; thermal conductivity
k'	0 (perfect gas), 1 (incompressible flow) in expression for H
M	moment
$\dot{m}$	mass flow rate
Nu	local Nusselt number ($= rq_s/(k(T_s - T_{s,ad}))$)
p	static pressure
Pr	Prandtl number ($= \mu c_p/k$)
Pr_t	turbulent Prandtl number
q_s	convective heat flux from disc to air
$\dot{Q}$	rate of heat transferred to fluid
r, ϕ, z	radial, tangential and axial coordinates
q	heat flux
R	recovery factor
Re_ϕ	rotational Reynolds number ($= \rho\Omega b^2/\mu$)
s	axial width of rotating cavity
T	temperature
U	total velocity
U_τ	friction velocity ($= \sqrt{\tau_w/\rho}$)
V_r, V_ϕ, V_z	time-averaged radial, circumferential, and axial components of velocity
$\dot{W}$	rate of work done by fluid
x	nondimensional radial coordinate ($= r/b$)
y	distance normal to the wall
y^+	nondimensional distance ($= \rho y U_\tau/\mu$)
α	ratio of pre-swirl ratios ($= \beta_p/\beta_{p,crit}$)
β	swirl ratio ($= V_\phi/\Omega r$)
β_p	pre-swirl ratio ($= V_{\phi,p}/\Omega r_p$)
Δr_b	radial width of blade-cooling slot
ε	turbulent energy dissipation rate
γ	ratio of specific heats ($= c_p/c_v$)
Γ	swirl ($= rV_\phi$)
λ_T	turbulent flow parameter ($= C_w/Re_\phi^{0.8}$)
μ	dynamic viscosity
ρ	density
Θ	nondimensional temperature difference
τ	shear stress
Ω	angular speed of disc

Superscript

1	bulk-average value

Subscripts

ad	adiabatic value
av	radially weighted average
b	blade-cooling air
crit	critical value (of β_p)
e	edge of source region
eff	effective value
fd	free-disc value
min	minimum value
o	total value in stationary frame of reference; value when $\beta_p = 0$
opt	optimal value (of β_p)
p	pre-swirl air
s	disc surface
t	total value in rotating frame of reference
∞	value in core outside boundary layers
$*$	value at stagnation point (where $\beta_\infty = 1$)
1	inlet to cavity (at radial location, and downstream, of pre-swirl nozzles)
2	outlet from cavity (at radial location, and downstream, of blade-cooling holes)

flow structure, and the ranges of these parameters cover values of interest to the gas-turbine designer. In addition to λ_T and β_p, Re_ϕ has a strong effect on the magnitude of the Nusselt numbers; in an engine, Re_ϕ is likely to be an order-of-magnitude larger than the values considered here, but that is thought unlikely to affect the flow structure or the main findings of this paper.

The steady-state, axisymmetric elliptic-flow solver described by Karabay et al. (1999) and Pilbrow et al. (1999) was used for the computations described here. The Morse (1988, 1991) low-Reynolds-number k–ϵ turbulence model, including modifications suggested by its author, was used to close the primitive-variable form of the Reynolds-averaged Navier–Stokes and energy equations, and the Launder and Sharma (1974) turbulence-model was used to provide initial values for the Morse model. Incompressible flow was assumed (which is appropriate for the ranges of the parameters considered here), and turbulent heat transfer was represented using a turbulent Prandtl number equal to 0.9 for air and 1 for the Reynolds analogy. The discretised finite-volume equations were solved using the SIMPLEC pressure-correction technique with multigrid convergence acceleration, and hybrid differencing was used to approximate convective fluxes.

A suitable angular speed, Ω, was used for the rotating surfaces to give the required rotational Reynolds number, Re_ϕ, and computations were carried out in a stationary reference frame. Uniform values of V_r and V_ϕ were prescribed at the radial inlet at $r = a$, in order to give the required inlet values of flow rate and pre-swirl ratio. Global continuity was ensured by prescribing a uniform axial velocity at the outlet, at $r = r_2$ in the right-hand disc. Zero normal-derivative conditions were used for the tangential velocity and fluid enthalpy at the outlet, allowing the total temperature of the "blade-cooling air" to be computed. The remaining velocity components at flow boundaries were taken to be zero, and no-slip conditions were used at solid surfaces. Both discs were given the same temperature profiles and a zero heat-flux condition was imposed at the outer-shroud surface.

Low-Reynolds-number k–ϵ turbulence models require a very fine grid near walls, and the 67×111 (axial and radial) grid used here satisfied the condition, suggested by Morse (1991, 1988) that $y+ < 0.5$ for the near-wall grid points. The grid expanded away from the walls as a geometric progression with expansion factors of around 1.22. Uniform spacing was used in the central region (see Fig. 2(b)), and the grid was refined in the region around $r = r_2$ so that eight points resolved the outlet slot in the disc. Computations were also carried out on a 93×111 grid, and the results suggested that the computations described below were not affected by the grid resolution. Computing times were around two CPU hours using a Silicon Graphics R10000 processor.

Further details are given by Karabay (1998) on whose thesis most of this paper is based.

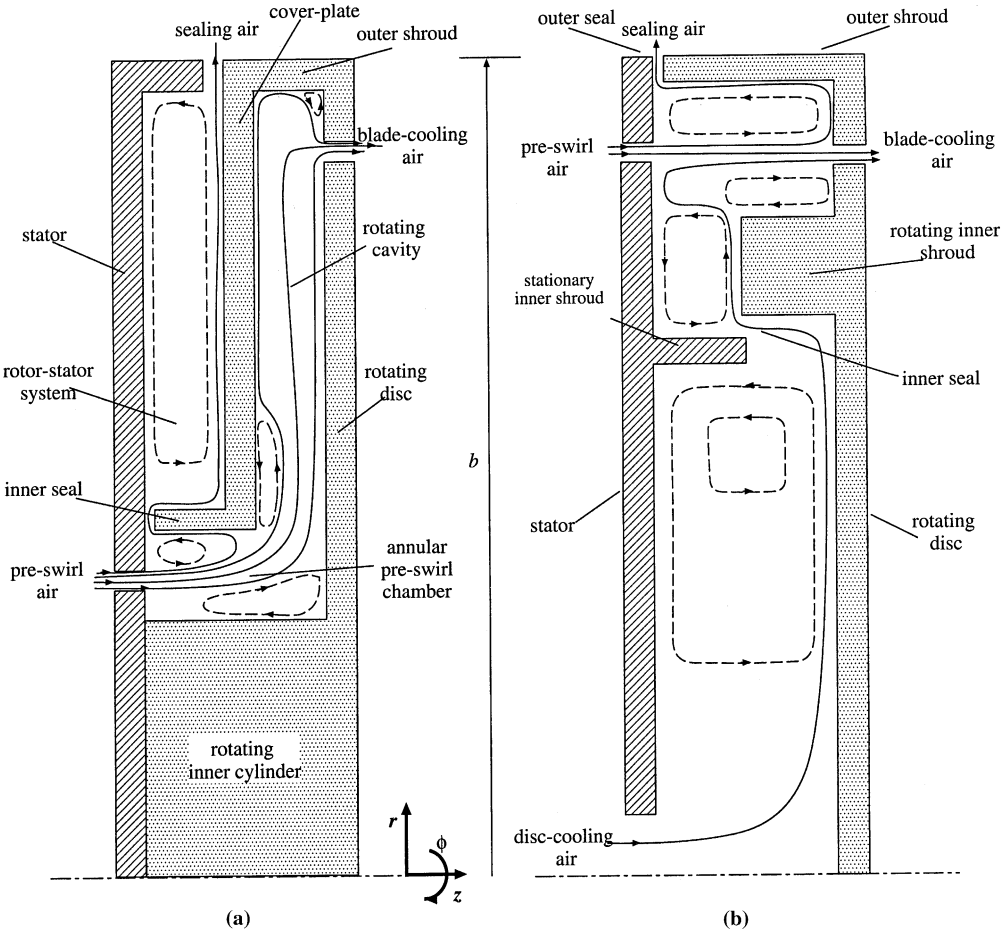

Fig. 1. Schematic diagram of pre-swirl systems: (a) cover-plate system; (b) direct-transfer system. (——) primary flow; (- - -) secondary flow; (▨) rotating; (▨) stationary.

3. Fluid dynamics of the rotating cavity

3.1. Theoretical flow structure

Owen and Rogers (1995) showed that, for a rotating cavity with a radial outflow of fluid, the flow structure is mainly controlled by two parameters, the pre-swirl ratio β_p and the turbulent flow parameter λ_T, both of which are defined in the nomenclature.

For sufficiently large values of λ_T, the flow inside the rotating cavity shown in Fig. 2 will behave as a free vortex. Under these conditions, $V_{\phi,\infty} \propto r^{-1}$, where $V_{\phi,\infty}$ is the tangential component of velocity outside the boundary layers on the rotating discs. As $V_{\phi,\infty} = \beta_p \Omega r$, at the outlet of the pre-swirl nozzles (where $r = r_1$), it follows that, for an ideal free vortex,

$$\frac{V_{\phi,\infty}}{\Omega r} = \beta_p \left(\frac{r_1}{r}\right)^2 = \beta_p \left(\frac{x_1}{x}\right)^2, \tag{3.1}$$

where x is the nondimensional radial coordinate. Of particular importance is the nondimensional radius, x_*, where $V_{\phi,\infty} = \Omega r_*$. It follows from Eq. (3.1) that

$$x_* = \beta_p^{1/2} x_1. \tag{3.2}$$

For a rotating flow in which the Coriolis forces dominate over the inertial forces, the flow in the boundary layers is radially inward when $V_{\phi,\infty} > \Omega r$ and outward when $V_{\phi,\infty} < \Omega r$. Thus there is a stagnation point on the rotating discs where $V_{\phi,\infty} = \Omega r$; this occurs where $x = x_*$, and for free-vortex flow x_* is given by Eq. (3.2).

Owen and Rogers solved the momentum-integral equations for swirling flow in a rotating cavity and computed values for the nondimensional extent of the source region, x_e. From these computed values, they obtained a correlation which, for the rotating cavity with radial outflow considered here, can be expressed as

$$\left(\frac{x_*}{x_e}\right)^{2.35} + \left(\frac{x_{e,0}}{x_e}\right)^{1.57} = 1, \tag{3.3}$$

where $x_{e,0}$ is the value of x_e when the flow enters without swirl ($\beta_p = 0$) and x_* is given by Eq. (3.2). It can be shown that

$$x_{e,0} = 1.375 \lambda_T^{5/13}. \tag{3.4}$$

Eq. (3.3) is only valid for cases where the source region does not fill the cavity, that is for $x_e < 1$. It is invalid for cases where β_p is so large that $V_{\phi,\infty} > \Omega r$ throughout the cavity as, under these conditions, the flow will always be radially inward in the boundary layers on the discs and recirculating flow will occur throughout the cavity. To ensure that $V_{\phi,\infty}/\Omega r$ is less than unity at $r = b$, it follows from Eq. (3.2) that $\beta_p x_1^2$ must be less than unity. With the proviso that $\beta_p x_1^2 < 1$, it can be shown using Eq. (3.3) that the source region will fill the cavity (that is, $x_e = 1$) when

$$\lambda_T = 0.437[1 - (\beta_p x_1^2)^{1.175}]^{1.656}. \tag{3.5}$$

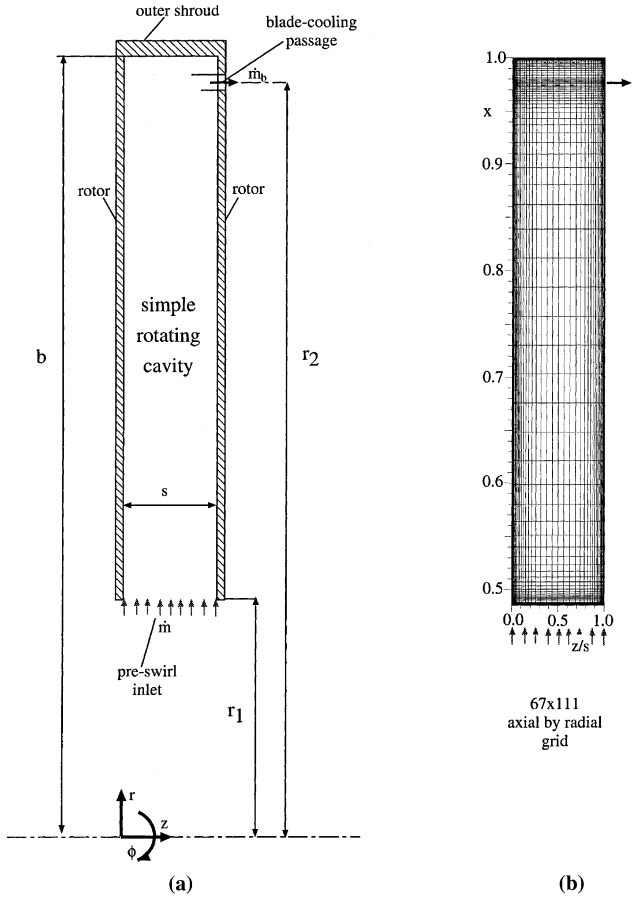

Fig. 2. (a) Schematic representation of the simple cavity; (b) grid distribution used in computation.

That is, free-vortex flow will occur throughout the cavity when λ_T exceeds the value given by Eq. (3.5); this is usually the case in most practical pre-swirl systems.

3.2. Computed flow structure

Fig. 3 shows the effect of λ_T and β_p on the computed streamlines in the rotating cavity for $Re_\phi = 0.903 \times 10^6$. Also shown, for $\beta_p > 1$, are the contours where $V_{\phi,\infty}/\Omega r = 1$ and the edges of the source region, given by Eq. (3.3), for those cases where $x_e < 1$.

Referring to the streamlines for $\lambda_T = 0.1$, the following observations can be made:

- For $\beta_p = 2$ and 3, recirculation occurs in a separation zone; the edge of this zone is at $x = 0.66$ for $\beta_p = 2$ and $x = 0.76$ for $\beta_p = 3$. These locations correspond to the point where $V_{\phi,\infty}/\Omega r = 1$ on the disc: this is consistent with the statement made in Section 3.1 that radial inflow occurs in the boundary layers when $V_{\phi,\infty}/\Omega r > 1$.
- For $\beta_p = 1$ and 2, Eq. (3.3) gives $x_e = 0.75$ and 0.89, respectively, which are consistent with the behaviour of the streamlines: for $x > x_e$, the flow stratifies and nonentraining Ekman-type layers are visible.

Eq. (3.5) implies that the source region should fill the cavity for $\lambda_T = 0.1$ and 0.4 when $\beta_p > 4$ and 0.35, respectively, and the computed streamlines shown in Fig. 3 are consistent with these results.

Computed velocities (not shown here) reveal that, outside the boundary layers on the disc, there is little axial variation of the tangential component of velocity, and $V_{\phi,\infty}/\Omega r$ is virtually invariant with z and depends mainly on r. Referring to Eq. (3.1), for an *ideal free vortex*, $V_{\phi,\infty}/\Omega r \propto x^{-2}$. It is therefore instructive to plot the computed values of $V_{\phi,\infty}/\Omega r$ against x^{-2}: a free vortex will appear as a straight line passing through the origin at $x^{-2} = 0$.

Fig. 4 shows the effects of λ_T and β_p on the computed variation of $V_{\phi,\infty}/\Omega r$ with x^{-2} (at the mid-axial plane, $z/s = 0.5$), for $Re_\phi = 0.903 \times 10^6$, together with the ideal free vortex according to Eq. (3.1) with $x_1 = 0.48$. Except for the results for $\beta_p = 0$, the computations approximate to free-vortex flow over most of the cavity, but the computed values of $V_{\phi,\infty}/\Omega r$ tend to be lower than those for the ideal free vortex. Experimental evidence for these free-vortex flows is given by Karabay et al. (1999, 2000) who used laser Doppler anemometry (LDA) to measure the velocities inside a pre-swirl rotating-disc rig.

By analogy with Eq. (3.1), *an effective free vortex* can be obtained using an *effective pre-swirl* ratio, $\beta_{p,eff}$, such that

$$\frac{V_{\phi,\infty}}{\Omega r} = \beta_{p,eff}\left(\frac{x_1}{x}\right)^2. \tag{3.6}$$

The effective free-vortex curves shown in Fig. 4 were obtained using the computed value of $V_{\phi,\infty}/\Omega r$ at a suitable radius: a value of $x = 0.67$ ($x^{-2} = 2.22$) was arbitrarily chosen. For $\beta_p > 0$, these curves show a good fit to the computed results over most of the cavity except near the inlet at $x_1 = 0.485$ ($x_1^{-2} = 4.24$) and near the periphery at $x = 1$. The results for $\lambda_T = 0.1$ and $\beta_p = 1$ show a departure between the effective free vortex and the computed values of $V_{\phi,\infty}/\Omega r$ at $x \approx 0.7$; this is where the source region ends and Ekman-type layers begin. This marks the end of free-vortex flow, and similar departures can be seen for $\beta_p = 1$ for all values of λ_T shown in the figure.

The effective free-vortex curves can be used in conjunction with Eq. (3.6) to calculate $\beta_{p,eff}$. The values determined in this way were found to depend strongly on β_p but varied only weakly with λ_T. The following correlation was obtained for $x_1 = 0.485$, $0.5 < \beta_p < 4$ and $0.1 < \lambda_T < 0.4$:

$$\beta_{p,eff} = 1.034\beta_p - 0.043\beta_p^2. \tag{3.7}$$

Fig. 5 shows the computed values of $\beta_{p,eff}$ together with the correlated variation given by Eq. (3.7), which provides a good fit to the computed values. The fact that $\beta_{p,eff} < \beta_p$ when $\beta_p > 1$ for the simple cavity is attributed to the recirculation region near the inlet. There is a transfer of angular momentum between the fluid flowing radially outwards in the core and that flowing inwards in the boundary layers on the discs. This transfer creates an initial loss of momentum in the core fluid; radially outward of the recirculation region, the angular momentum of the core fluid is conserved, which results in a free vortex with an effective swirl ratio lower than that at inlet. The size of the recirculation region and the size of the losses increase as β_p increases; this loss mechanism appears to be only weakly affected by λ_T, but it is expected to depend on the inlet geometry.

Karabay et al. (2000) presented measurements for $\beta_{p,eff}$ obtained for the "whole pre-swirl rotating-disc system" (see Fig. 1(a)) in which there is an axial flow into the rotating cavity. Their empirical correlation, which agreed closely with their computations for the whole system, is also plotted in Fig. 5. The fact that the experimental values of $\beta_{p,eff}$ are smaller than those given by Eq. (3.7) is attributed to the increased losses that occur in the whole system with an axial inlet compared with those for the simple cavity in which the flow enters radially.

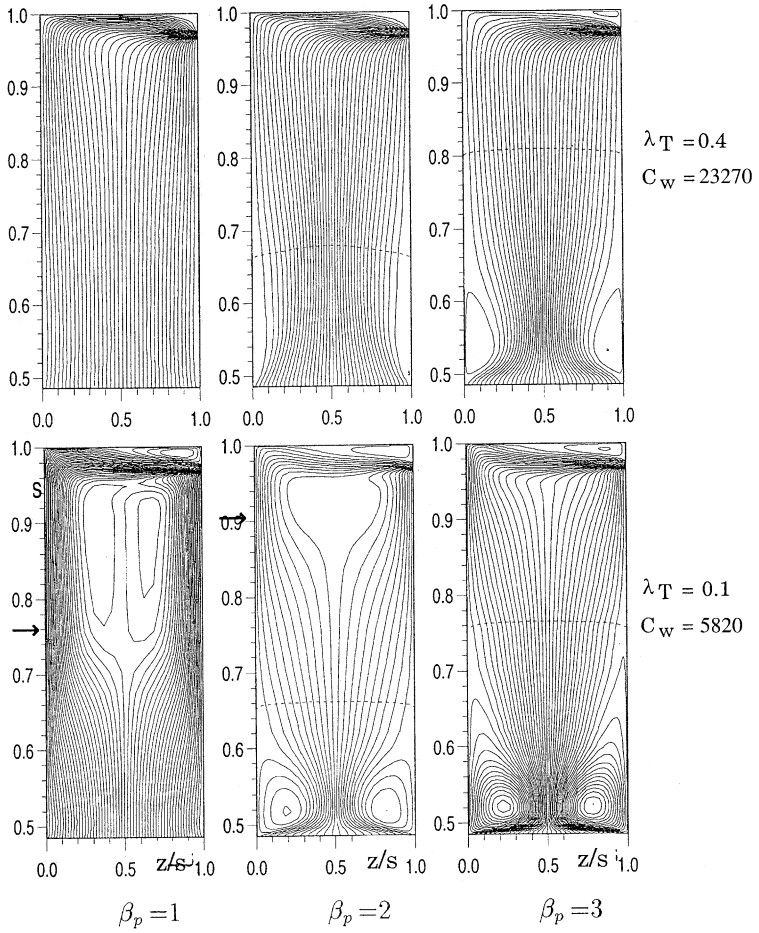

Fig. 3. Effect of varying β_p and λ_T on computed streamlines with $Re_\phi = 0.903 \times 10^6$: (- - -) $\beta = 1$; (→) end of the source region (Eq. (3.3)).

3.3. Calculated pressure distribution

The flow in the core outside the boundary layers is considered to be inviscid, and the velocity and pressures are assumed to depend only on the radius. The Navier–Stokes equations then reduce to

$$\frac{1}{\rho}\frac{\mathrm{d}p}{\mathrm{d}r} = \frac{V_{\phi,\infty}^2}{r} - V_{r,\infty}\frac{\mathrm{d}V_{r,\infty}}{\mathrm{d}r}. \tag{3.8}$$

For free-vortex flow in the core, where $V_{\phi,\infty} \propto r^{-1}$, it follows that:

$$\frac{1}{\rho}\frac{\mathrm{d}p}{\mathrm{d}r} = -\frac{1}{2}\frac{\mathrm{d}}{\mathrm{d}r}(V_{\phi,\infty}^2 + V_{r,\infty}^2). \tag{3.9}$$

For an adiabatic perfect gas, where p/ρ^γ is constant, the left-hand side of Eq. (3.9) can be integrated from $r = r_1$, the inner radius of the cavity ($r_1 = a$), where $p = p_1$, such that

$$\int_{r_1}^{r}\frac{1}{\rho}\frac{\mathrm{d}p}{\mathrm{d}r}\,\mathrm{d}r = \left(\frac{\gamma}{\gamma-1}\right)\frac{p_1}{\rho_1}\left\{\left(\frac{p}{\rho}\right)^{(\gamma-1)/\gamma} - 1\right\}. \tag{3.10}$$

The local pressure coefficient, C_p, can be defined as

$$C_p = \left(\frac{\gamma}{\gamma-1}\right)\frac{p_1}{(1/2)\rho_1\Omega^2 r_1^2}\left\{\left(\frac{p}{\rho}\right)^{(\gamma-1)/\gamma} - 1\right\}. \tag{3.11}$$

In the limit as $p \to p_1$, Eq. (3.11) reduces to the incompressible form

$$C_p = \frac{p - p_1}{(1/2)\rho_1\Omega^2 r_1^2}. \tag{3.12}$$

Eq. (3.9) can be integrated to give

$$C_p = \frac{(V_{\phi,\infty}^2 + V_{r,\infty}^2)_1 - (V_{\phi,\infty}^2 + V_{r,\infty}^2)_2}{\Omega^2 r_1^2}, \tag{3.13}$$

where the radial component of velocity can be approximated by

$$V_{r,\infty} = \frac{\dot{m}}{2\pi\rho r s} \tag{3.14}$$

or, in nondimensional form,

$$\frac{V_{r,\infty}}{\Omega r} = \frac{C_w}{2\pi G Re_\phi}\frac{b^2}{r_1 r}. \tag{3.15}$$

Using this equation, together with Eq. (3.6), in (3.13) gives

$$C_p = \left\{\beta_{p,\mathrm{eff}}^2 + \left(\frac{\lambda_T}{2\pi G Re_\phi^{0.2}}\right)^2\left(\frac{b}{r_1}\right)^4\right\}\left\{1 - \left(\frac{r_1}{r}\right)^2\right\}, \tag{3.16}$$

where $\beta_{p,\mathrm{eff}}$ can be calculated from Eq. (3.7).

Fig. 6 shows comparisons between Eq. (3.16) and the computed radial variation of C_p for $Re_\phi = 0.9 \times 10^6$, $\lambda_T = 0.1, 0.22$, and 0.4, and $\beta_p = 1$, 2 and 3. The effect of λ_T is relatively weak, and C_p is controlled principally by $\beta_{p,\mathrm{eff}}$ (and hence by β_p) for the conditions used here.

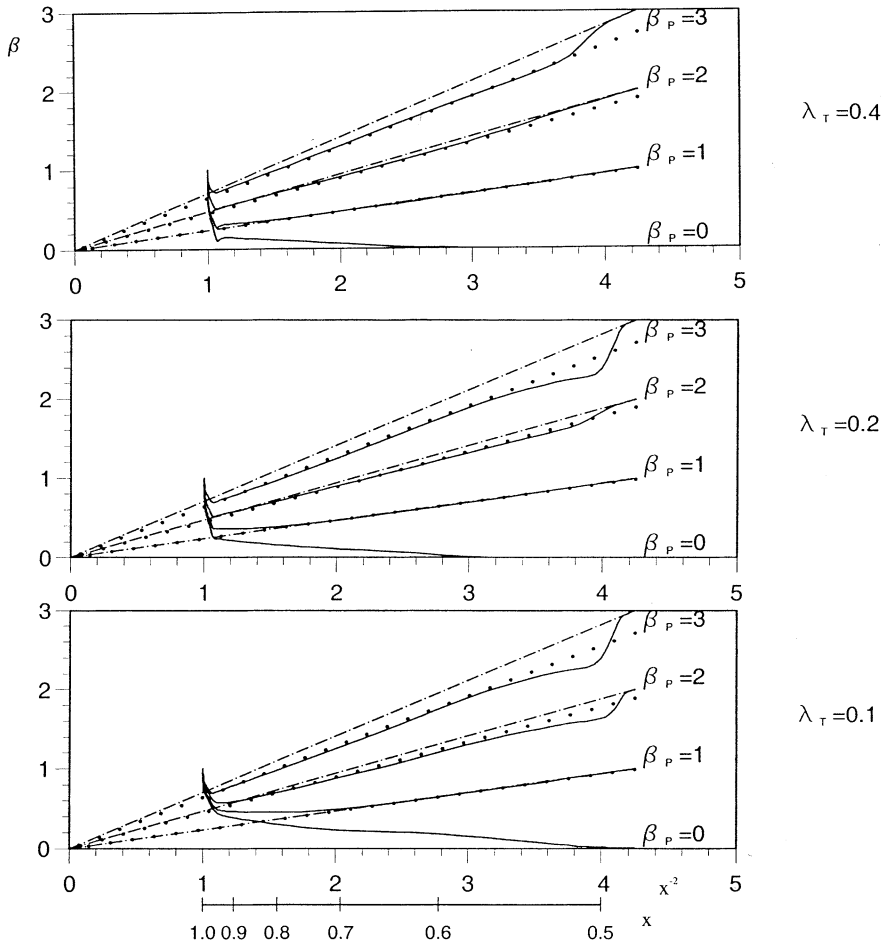

Fig. 4. Computed variation of $V_{\phi,\infty}/\Omega r$ with x^{-2} for $Re_\phi = 0.903 \times 10^6$; (–·–·–) ideal free vortex; (···) effective free vortex; (——) computations.

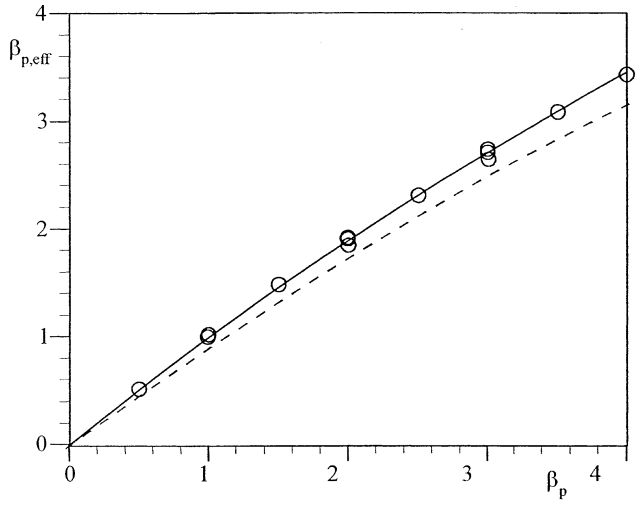

Fig. 5. Computed and correlated variation of $\beta_{p,eff}$ with β_p: (◯) computed values; (–) Eq. (3.7); (- - -) empirical correlation of Karabay et al. (2000).

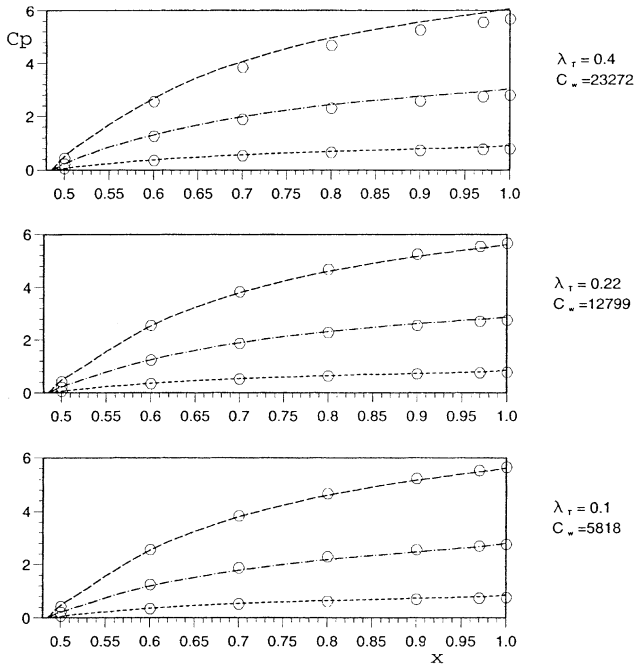

Fig. 6. Effect of λ_T on computed and calculated pressure coefficients for $Re_\phi = 0.903 \times 10^6$. Computation: (- - -) $\beta_p = 1$; (–·–·–) $\beta_p = 2$; (– –) $\beta_p = 3$. Calculation (Eq. (3.16)): ◯.

4. Thermodynamics of pre-swirl systems

For this analysis, station 1 is the inlet to the simple cavity at $r_1 = r_p = a$, 2 is inside the blade-cooling passages at the outlet

of the cavity at $r_2 = r_b$, and the velocities and temperatures at stations 1 and 2 are bulk-average values.

The steady-flow energy equation for the system can be written as

$$\dot{Q}_{12} - \dot{W}_{12} = \dot{m} c_p (T_{0,2} - T_{0,1}), \tag{4.1}$$

where $\dot{Q}_{12}$ is the rate of heat transferred to the air between stations 1 and 2, $\dot{W}_{12}$ the rate of work done by the air, $\dot{m}_b$ the mass flow rate of the air, and $T_{0,1}$ and $T_{0,2}$ are the total temperatures of the air at stations 1 and 2 in a *stationary* frame of reference.

If Ω is the angular speed of the rotating cavity and M is the moment exerted by the air on the rotating surfaces, then

$$\dot{W}_{12} = M\Omega. \tag{4.2}$$

As M is equal to the rate of change of angular momentum of the air, it follows that:

$$\dot{W}_{12} = -\dot{m}\Omega(r_2 V_{\phi,2} - r_1 V_{\phi,1}), \tag{4.3}$$

where

$$V_{\phi 1} = \beta_p \Omega r_1 \tag{4.4}$$

and

$$V_{\phi 2} = \Omega r_2. \tag{4.5}$$

Eq. (4.1) can then be rewritten as

$$c_p(T_{0,2} - T_{0,1}) = \frac{\dot{Q}_{12}}{\dot{m}} + \Omega^2 r_2^2 \left(1 - \beta_p \frac{r_1^2}{r_2^2}\right). \tag{4.6}$$

In the *stationary frame*, the total temperature, $T_{0,2}$, can be written for a perfect gas as

$$c_p T_{0,2} = c_p T_2 + \tfrac{1}{2}(V_r^2 + V_\phi^2 + V_z^2)_2, \tag{4.7}$$

where T_2 is the static temperature at the outlet. It is more appropriate, however, to use $T_{t,2}$, the total temperature in the *rotating frame*, which is the value that would be measured by a total-temperature probe located in a blade-cooling passage where $V_{\phi,2} = \Omega r_2$. It is this value that controls the heat transfer from the turbine blades to the cooling air. (Eq. (4.5) implies that the air inside the cooling passage is in solid-body rotation at $r = r_2$. In general, immediately upstream of the passage, $V_\phi \neq \Omega r_2$; additional work is done on, or by, the air inside the passage until solid-body rotation is achieved at some downstream location. Consequently, as Karabay et al. (2000) pointed out, the accurate measurement of T_{t2} is difficult to achieve. For the computations discussed below, the "additional work" was added to the computed total temperature.)

By definition

$$c_p T_{t,2} = c_p T_2 + \tfrac{1}{2}(V_r^2 + V_z^2)_2 \tag{4.8}$$

and it follows that:

$$c_p T_{t,2} = c_p T_{0,2} - \tfrac{1}{2}\Omega^2 r_2^2. \tag{4.9}$$

For consistency with Karabay et al. (1999), the blade-cooling effectiveness, Θ_b, is defined as

$$\Theta_b = \frac{c_p(T_{0,1} - T_{t,2})}{(1/2)\Omega^2 r_2^2}. \tag{4.10}$$

This is the nondimensional temperature difference between the stationary pre-swirl nozzles and the rotating blade-cooling passages, and a positive value of Θ_b signifies that the pre-swirl system is effective in reducing the total temperature of the cooling air.

Using Eqs. (4.9) and (4.10), Eq. (4.6) can be rewritten as

$$\Theta_b = 2\frac{r_1^2}{r_2^2}\beta_p - 1 - \frac{\dot{Q}_{12}}{(1/2)\dot{m}\Omega^2 r_2^2}. \tag{4.11}$$

For the adiabatic case, where $\dot{Q}_{12} = 0$ and $\Theta_b = \Theta_{b,ad}$, Eq. (4.11) reduces to

$$\Theta_{b,ad} = 2\frac{r_1^2}{r_2^2}\beta_p - 1, \tag{4.12}$$

which is the result obtained by Karabay et al. (1999). This shows that, for a given value of T_{01} in an adiabatic system, T_{t2} decreases as β_p increases.

Fig. 7 shows a comparison between the computed values of $\Theta_{b,ad}$ for the simple cavity, using the solver described in Section 2, and the variation given by Eq. (4.12) for $r_1/r_2 = 0.5$. As Eq. (4.12) is exact, any differences between this equation and the computation are caused by numerical errors; it can be seen from Fig. 7 that these errors are small. (It should be noted that, in a gas turbine the dynamic temperature, $(1/2)\Omega^2 r_2^2/c_p$, can be around 50°C, and so the accurate determination of $\Theta_{b,ad}$ is important for the design of cooling-air systems.)

In general, heat may be transferred to the cooling air from all bounding surfaces. In the experiments of Pilbrow et al. (1999), the principal heat transfer was from the heated disc, and the other surfaces were quasi-adiabatic. It is therefore convenient to define the average Nusselt number, Nu_{av}, as

$$Nu_{av} = \frac{q_{s,av} b}{k(T_s - T_{s,ad})_{av}}, \tag{4.13}$$

where

$$q_{s,av} = \frac{\dot{Q}_{12}}{\pi(b^2 - a^2)}. \tag{4.14}$$

a and b being the inner and outer radii of the heated disc, and the subscript 'av' referring to the radially-weighted average. (For the case where the cover-plate and shroud are not adiabatic, Eq. (4.13) would have to take account of the heat transfer from these surfaces.) The adiabatic-disc temperature, $T_{s,ad}$, is defined in Section 5.

It is also convenient to define

$$\Theta_{s,av} = \frac{c_p(T_s - T_{s,ad})_{av}}{(1/2)\Omega^2 r_2^2}. \tag{4.15}$$

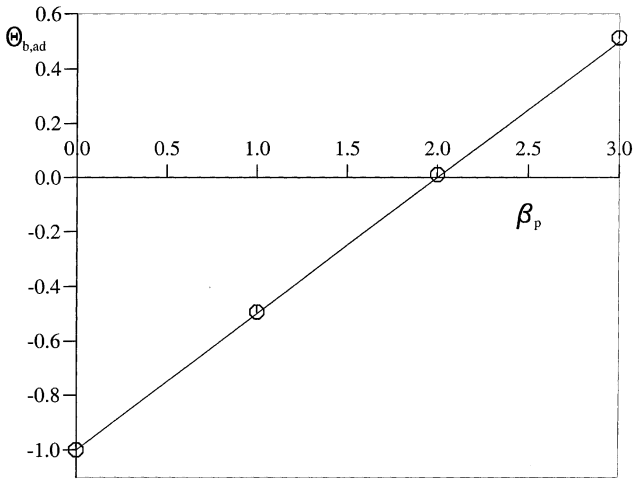

Fig. 7. Comparison between computed and theoretical variation of $\Theta_{b,ad}$ with β_p for $r_1/r_2 = 0.5$, $Re_\phi = 0.903 \times 10^6$, $\lambda_T = 0.3$: (——) Eq. (4.12); (○) computed values.

Using this definition, Eq. (4.11) becomes

$$\Theta_b = \Theta_{b,ad} - \pi\left(1 - \frac{a^2}{b^2}\right)\frac{Nu_{av}}{PrC_w}\Theta_{s,av}, \tag{4.16}$$

where Pr is the Prandtl number of the fluid.

In order to use Eq. (4.16) to find ΔT, where $\Delta T = T_{t,2} - T_{0,1}$, it is necessary to know Nu_{av} and $\Theta_{s,av}$, which depend on the geometry of the pre-swirl system and on the thermal and flow conditions. The Reynolds analogy can be used to address this problem, as discussed below.

5. Heat transfer: application of the Reynolds analogy to free-vortex flows

Considerable insight into the relationship between the flow and heat transfer in a rotating cavity can be given by the Reynolds analogy, the salient details of which are given in Appendix A. Of interest here are the relationships between the heat flux and the shear stress, and between the average Nusselt number and the moment coefficient, for the special case where there is a free vortex in the core outside the boundary layers on the rotating discs. The definition of the adiabatic-disc temperature is particularly important for pre-swirl rotating-disc systems, as discussed below.

5.1. Adiabatic-disc temperature

The adiabatic disc-temperature given, for $Pr = 1$, in Appendix A can be extended to the case where $Pr \neq 1$ by the use of a recovery factor, R. Eqs. (A.11a) and (A.11b) can be, respectively, written as

$$T_{s,ad} = T_\infty + R\frac{\Omega^2 r^2}{2c_p}\left(1 - \frac{V_{\phi,\infty}}{\Omega r}\right)^2 \tag{5.1a}$$

and

$$T_{s,ad} = T_{s,*} + R\frac{\Omega^2 r^2}{2c_p}\left(1 - \frac{r_*^2}{r^2}\right). \tag{5.1b}$$

Eq. (5.1a) is the same as that used by Chew and Rogers (1988), which is a generalisation of the result derived by Owen (1971). The recovery factor is assumed to be a function of the Prandtl number, and $R = 1$ when $Pr = 1$. In the literature, it is customary to assume that $R = Pr^{1/3}$ for fluids with Prandtl numbers of the order of unity; for air, with $Pr = 0.71$, this gives $R = 0.892$.

As, in general, T_∞ and $T_{s,*}$ are unknown, it is convenient to express Eqs. (5.1a) and (5.1b) in terms of $T_{0,1}$, which is usually known. This can be done using either

$$T_{0,1} = T_\infty + \frac{V_{\phi,\infty}^2}{2c_p} \tag{5.2a}$$

or

$$T_{0,1} = T_{s,*} + \frac{\Omega^2 r_*^2}{2c_p}. \tag{5.2b}$$

With the use of Eqs. (3.1) and (3.2), Eqs. (5.1a) and (5.1b) can be, respectively, expressed as

$$T_{s,ad} - T_{0,1} = \frac{\Omega^2 b^2}{2c_p}\{Rx^2 - (1-R)\beta_p^2 x_1^4 x^{-2} - 2R\beta_p x_1^2\} \tag{5.3a}$$

and

$$T_{s,ad} - T_{0,1} = \frac{\Omega^2 b^2}{2c_p}\{Rx^2 - (1+R)\beta_p x_1^2\}. \tag{5.3b}$$

For $R = 1$ or $\beta_p = 0$, Eqs. (5.3a) and (5.3b) are identical.

Fig. 8 shows comparisons between Eqs. (5.3a) and (5.3b) and the computed adiabatic-disc temperatures for $Re_\phi = 0.906 \times 10^6$ and $\lambda_T = 0.3$. In Fig. 8(a), where $Pr = R = 1$, the agreement between the theoretical and computed results is very good. In Fig. 8(b), where $Pr = 0.71$ and $R = 0.892$, the agreement between Eq. (5.3a) and the computations is again very good, but Eq. (5.3b) diverges from the computations, and from Eq. (5.3a), as β_p increases and as x^2 decreases.

For flow over a stationary surface, where the free-stream velocity is U_∞, the recovery factor is often regarded as the ratio of the "frictional temperature" increase, $T_{s,ad} - T_\infty$, to the "adiabatic compression", $U_\infty^2/2c_p$. In a rotating frame of reference, U_∞^2 could be replaced by $(\Omega r - V_{\phi,\infty})^2$, in which case the recovery factor used in Eq. (5.1a) is consistent with that for a stationary surface. In the authors' earlier publications, Eq. (5.3b) was used for the adiabatic-disc temperature. In the future, Eq. (5.3a) will be used, although the differences in the evaluated Nusselt numbers are likely to be very small.

5.2. Local Nusselt numbers

Any temperature difference, ΔT say, can be used in the definition of the Nusselt number, but there will be an inconsistency unless $q_s = 0$ when $\Delta T = 0$; the only consistent definition is where $\Delta T = T_s - T_{s,ad}$. It should also be noted that, for engine operating conditions, the magnitude of the right-hand side of Eqs. (5.3a) and (5.3b) can be around 50°C: there can be a significant difference between the use of $T_{0,1}$ (which the unwary may choose) and $T_{s,ad}$ (which is used here).

For $Pr = 1$, Eqs. (A.10b) and (A.11b) in Appendix A can be combined to give

$$\frac{q_s}{\tau_{\phi,s}} = -\frac{c_p(T_s - T_{s,ad})}{\Omega r(1 - r_*^2/r^2)}. \tag{5.4}$$

The local Nusselt number is defined as

$$Nu = \frac{rq_s}{k(T_s - T_{s,ad})} \tag{5.5}$$

and it follows from Eqs. (5.4) and (3.2) that:

$$\begin{aligned} Nu &= -Re_\phi \frac{\tau_{\phi,s}}{\rho\Omega^2 b^2}\frac{1}{1 - x_*^2/x^2} \\ &= -Re_\phi \frac{\tau_{\phi,s}}{\rho\Omega^2 b^2}\frac{1}{1 - \beta_p x_1^2/x^2}. \end{aligned} \tag{5.6}$$

Fig. 9 shows comparisons between the computed local Nusselt numbers, for $0 \leqslant \beta_p \leqslant 3$ and $Pr = 1$, and those obtained from the Reynolds analogy. The latter values of Nu were calculated from Eq. (5.6) using the computed values of $\tau_{\phi,s}$ and, for $\beta_p > 1$, the value of x_*^2 was calculated from Eq. (3.2). The computations were obtained for the conditions given in Fig. 8, and the surface temperatures on the disc correspond to the quadratic distributions necessary for the Reynolds analogy (see Eq. (A.3)).

It can be seen that, apart from the results near $x = x_*$, the agreement between the computed Nusselt numbers and those obtained from the Reynolds analogy is mainly very good. (The shear stress $\tau_{\phi,s}$ is greater than or less than zero when x is, respectively, less than or greater than x_*, and there is a singularity in the right-hand side of Eq. (5.6) when $x^2 = x_*^2 = \beta_p x_1^2$. Accurate computations of Nu are difficult to achieve in this region.)

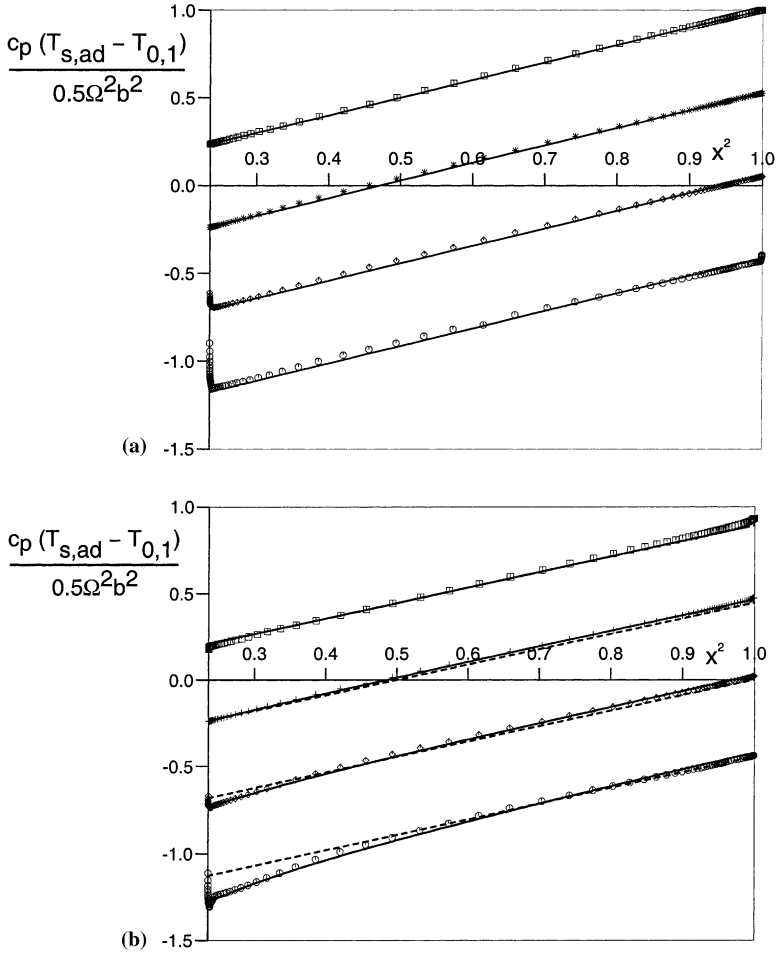

Fig. 8. Comparison between computational and theoretical adiabatic disc temperature for $Re_\phi = 0.903 \times 10^6$, $C_w = 17454$: (a) $Pr = 1$; (b) $Pr = 0.71$. Computations: (□) $\beta_p = 0$; (+) $\beta_p = 1$; (◇) $\beta_p = 2$; (○) $\beta_p = 3$; (——) Eq. (5.3a); (- - -) Eq. (5.3b).

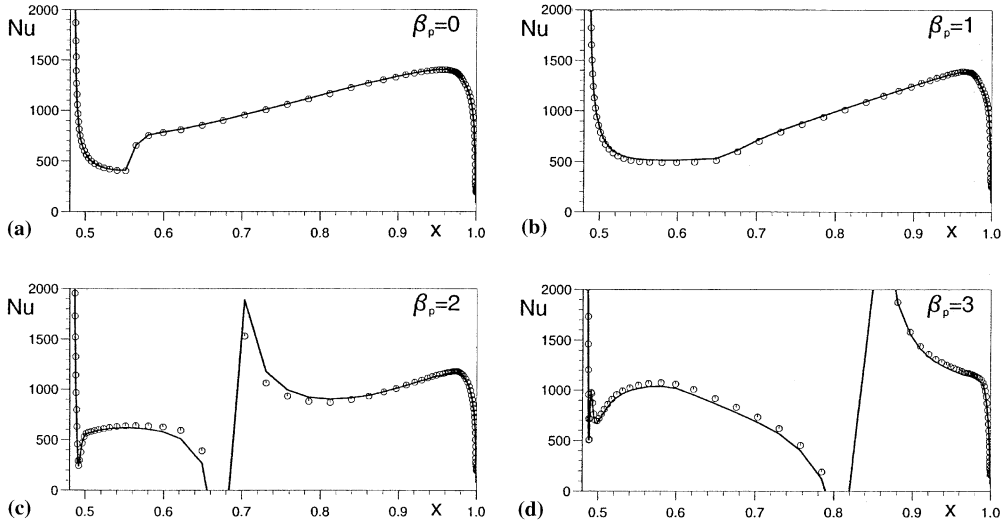

Fig. 9. Comparison between computed and theoretical local Nusselt numbers for $Pr = 1$, $Re_\phi = 0.903 \times 10^6$ and $\lambda_T = 0.3$. Computed values: ○; Eq. (5.6): ——.

5.3. Average Nusselt numbers

The temperature of the blade-cooling air is strongly affected by the average Nusselt number, Nu_{av}, as Eq. (4.16) shows, and the Reynolds analogy (for $Pr = 1$) can be used to derive an expression for Nu_{av}.

From Eq. (5.4)

$$q_{s,av} = \frac{2}{b^2 - a^2}\int_a^b r q_s \, dr = \frac{-2c_p}{\Omega(b^2 - a^2)}\int_a^b \frac{r^2 \tau_{\phi,s}(T_s - T_{s,ad})}{r^2 - r_*^2}\, dr. \tag{5.7}$$

From Eq.(A.3) in Appendix A

$$T_s - T_{s,*} = \frac{\Omega^2}{c_p}\left(C - \frac{1}{2}\right)(r^2 - r_*^2), \tag{5.8}$$

where for a perfect gas, C is an arbitrary constant. Using Eq. (A.11b) it follows that:

$$T_s - T_{s,ad} = \frac{\Omega^2}{c_p}(C - 1)(r^2 - r_*^2). \tag{5.9}$$

Hence, from Eq. (5.7)

$$q_{s,av} = -\frac{2\Omega}{b^2 - a^2}(C - 1)\int_a^b r^2 \tau_{\phi,s}\, dr. \tag{5.10}$$

Also

$$(T_s - T_{s,ad})_{av} = \frac{2}{b^2 - a^2}\int_a^b r(T_s - T_{s,ad})\, dr = \frac{2\Omega^2(C-1)}{c_p(b^2 - a^2)}\left\{\frac{b^4 - a^4}{4} - r_*^2\frac{(b^2 - a^2)}{2}\right\}. \tag{5.11}$$

Hence, using Eqs. (3.2), (5.10) and (5.11) in Eq. (4.13), it follows that:

$$Nu_{av} = \frac{Re_\phi C_m}{\pi(1 - (a^2/b^2))\{1 + (a^2/b^2) - 2\beta_p(r_1^2/b^2)\}}, \tag{5.12}$$

where C_m is the moment coefficient for the rotating disc, which is given by

$$C_m = \frac{-2\pi\int_a^b r^2 \tau_{\phi,s}\, dr}{(1/2)\rho\Omega^2 b^5}. \tag{5.13}$$

It should be noted that $\tau_{\phi,s}$ is negative when $V_{\phi,\infty} < \Omega r$ (that is, when $x > x_*$), and vice versa.

Substituting Eqs. (4.12), (5.9) and (5.12) into Eq. (4.16) gives

$$\Theta_b = \left\{2\frac{r_1^2}{r_2^2}\beta_p - 1\right\} - \left\{4(C-1)\frac{b^2}{r_2^2}\frac{Re_\phi C_m}{C_w}\right\}, \tag{5.14}$$

where Θ_b is the nondimensional difference in the total temperature of the blade-cooling air, as defined in Eq. (4.10).

6. Effect of β_p on disc moments and heat transfer for free-vortex flows

6.1. Moment coefficients

Knowing something, theoretically or experimentally, about the fluid mechanics, the engineer usually employs the Reynolds analogy to predict something about the heat transfer. For example, if the moment coefficient were known, the average Nusselt number could be estimated. However, Eq. (5.12) can be used to give insight into the fluid mechanics itself: in particular, it provides useful information about C_m.

It is reasonable to assume that Nu_{av} must always be a finite quantity: referring to Eq. (4.13), if Nu_{av} were infinite, then the average heat flux, $q_{s,av}$, would also be infinite for any nonzero value of the average temperature difference, $(T_s - T_{s,ad})_{av}$. Referring to Eq. (5.12), if Nu_{av} is to remain finite then C_m must equal zero when the denominator is zero. It is convenient to define a critical pre-swirl ratio, $\beta_{p,crit}$, such that $C_m = 0$ when $\beta_p = \beta_{p,crit}$, and it follows that:

$$\beta_{p,crit} = \frac{a^2 + b^2}{2r_1^2}. \tag{6.1}$$

(From Eq. (3.2), this occurs when $r_*^2 = 1/2(a^2 + b^2)$.)

Eq. (6.1) is a logical consequence of Eq. (5.12). Eq. (5.12) was derived from the Reynolds analogy, which is only strictly valid when the conditions stated in Appendix A are satisfied. However, as Eq. (5.13) shows, C_m depends on $\tau_{\phi,s}$, which in turn depends on the fluid dynamics and not, apart from any minor effects of property variations in the fluid, on the heat transfer. Therefore, if the statement that $C_m = 0$ when $\beta_p = \beta_{p,crit}$ is true when the Reynolds-analogy conditions apply, it must also be true when they do not apply. Consequently, Eq. (6.1) is valid regardless of the Prandtl number of the fluid or the thermal conditions of the flow. In particular, $\beta_{p,crit}$ depends only on the geometry (a, b and r_1) and not on the flow parameters (Re_ϕ, λ_T). *Paradoxically, despite the assumptions made in its derivation*, Eq. (6.1) *is generally valid for a rotating cavity in which there is free-vortex flow in the core.*

Eq. (5.12) can now be rewritten as

$$Nu_{av} = \frac{1}{\pi(1 - a^4/b^4)}\frac{Re_\phi C_m}{(1 - \beta_p/\beta_{p,crit})}. \tag{6.2}$$

For the cavity considered here, where $a = r_1 = 100$ mm and $b = 206$ mm, Eq. (6.1) gives $\beta_{p,crit} = 2.622$. Fig. 10 shows the computed variation of $C_m/C_{m,0}$ with $\beta_p/\beta_{p,crit}$, where $C_{m,0}$ is the value of C_m when $\beta_p = 0$ and $\beta_{p,crit} = 2.622$. These computations, which were made for $Re_\phi = 0.903 \times 10^6$ and $\lambda_T = 0.3$, are consistent with the value of $\beta_{p,crit}$ given by Eq. (6.1). Computations conducted at other values of Re_ϕ and λ_T confirmed that these flow parameters do not affect the value of $\beta_{p,crit}$.

It is convenient to correlate the moment coefficient by a polynomial of the form

$$C_m/C_{m,0} = 1 + A_1\alpha + A_2\alpha^2 + A_3\alpha^3 + \cdots \tag{6.3}$$

where α is the "ratio of the pre-swirl ratios" given by

$$\alpha = \beta_p/\beta_{p,crit} \tag{6.4}$$

and A_1, A_2, A_3 etc. are coefficients, which are expected to be functions of Re_ϕ and λ_T. Fig. 10 shows the linear variation where

$$C_m/C_{m,0} = 1 - \alpha \tag{6.5}$$

and the cubic variation where

$$C_m/C_{m,0} = 1 - 1.3582\alpha + 0.6035\alpha^2 - 0.2453\alpha^3. \tag{6.6}$$

In both cases, $C_m/C_{m,0} = 0$ when $\alpha = 1$. The cubic curve provides a good fit to the computed results; the linear variation is reasonable but, as discussed below, it has disadvantages when used in Eq. (6.2) to calculate the average Nusselt numbers.

6.2. Average Nusselt numbers

Fig. 11 shows the variation of Nu_{av} with $\beta_{p,crit}$ for $Re_\phi = 0.903 \times 10^6$ and $\lambda_T = 0.3$; for the computations, $Pr = 1$ and the

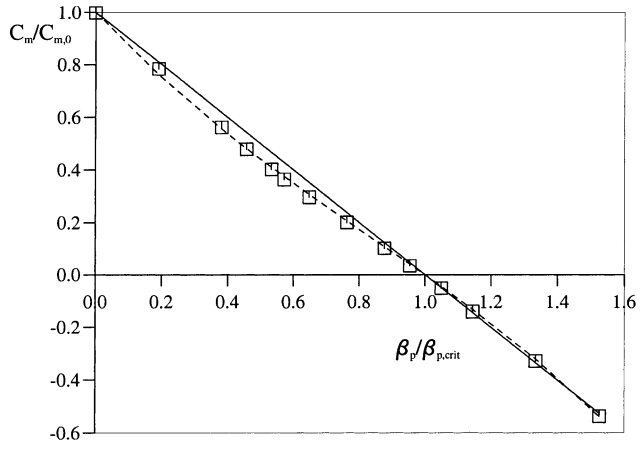

Fig. 10. Variation of $C_m/C_{m,0}$ with $\beta_p/\beta_{p,crit}$ for $Re_\phi = 0.903 \times 10^6$ and $\lambda_T = 0.3$. (□) computed values; (——) linear fit (Eq. (6.5)); (- - -) cubic fit (Eq. (6.6)).

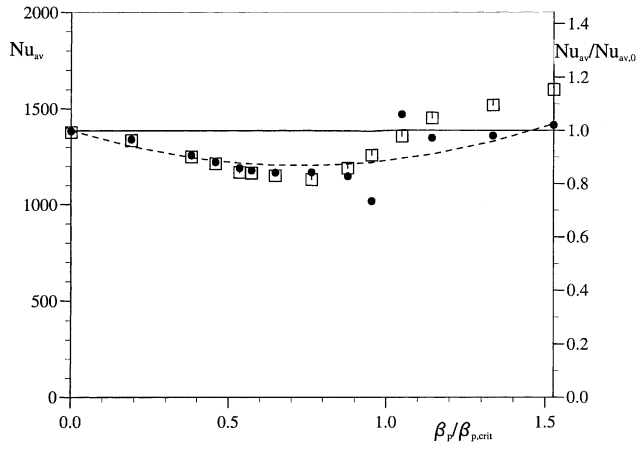

Fig. 11. Computed variation of Nu_{av} with $\beta_p/\beta_{p,crit}$ for $Pr = 1$, $Re_\phi = 0.903 \times 10^6$ and $\lambda_T = 0.3$. (□) Nu_{av}(i); (●) Nu_{av}(ii); (——) Nu_{av}(iii); (- - -) Nu_{av}(iv).

thermal boundary conditions satisfied the Reynolds analogy. Four methods were used to determine Nu_{av}.

(i) Nu_{av}(i). The local heat flux, q_s, computed from the energy equation, was integrated to calculate Nu_{av} from Eq. (4.13).
(ii) Nu_{av}(ii). The computed value of C_m was used in the Reynolds analogy, Eq. (6.2), to determine Nu_{av}.
(iii) Nu_{av}(iii). The linear fit to C_m (Eq. (6.5)) was used in the Reynolds analogy.
(iv) Nu_{av}(iv). The cubic fit to C_m (Eq. (6.6)) was used in the Reynolds analogy.

Referring to Fig. 11, the following points may be noted:

- For $\beta_p/\beta_{p,crit} \leqslant 0.76$ (that is, $\beta_p < 2$), Nu_{av}(i) and Nu_{av}(ii) are in good agreement, and both reduce as β_p increases.
- For $\beta_p/\beta_{p,crit} > 0.76$, the agreement between Nu_{av}(i) and Nu_{av}(ii) is not so good. The main reason for this is the singularity in Eq. (6.2) at $\beta_p/\beta_{p,crit} = 1$: small errors in the computed values of C_m cause large errors in Nu_{av}(ii). Also, as stated in Appendix A, the Reynolds analogy is strictly valid only for parabolic flows: as β_p increases, the recirculation region becomes larger and the flow becomes increasingly elliptic. It is considered to be this effect that causes Nu_{av}(ii) to diverge from Nu_{av}(i) at the larger values of β_p.
- Nu_{av}(iii) is invariant with β_p.
- Nu_{av}(iv) is in good agreement with Nu_{av}(ii) except, for the reasons given above, near the singularity at $\beta_p/\beta_{p,crit} = 1$. The large differences between Nu_{av}(iii) and Nu_{av}(iv), caused by small differences in C_m (see Fig. 10), show that this is an ill-conditioned problem.

Apart from Nu_{av}(iii), the computations show that there is a minimum value of Nu_{av} at some value of β_p. This value will be referred to as $\beta_{p,opt}$, the optimal pre-swirl ratio at which Nu_{av} is a minimum. For Nu_{av}(iii), $\beta_{p,opt} \approx 1.9$, which corresponds to

$$\beta_{p,opt}/\beta_{p,crit} \approx 0.73, \tag{6.7}$$

where $\beta_{p,crit}$ is given by Eq. (6.1).

Karabay (1998) conducted computations for air ($Pr = 0.71$) and for $0.42 \times 10^6 < Re_\phi < 0.9 \times 10^6$, $0.22 < \lambda_T < 0.4$, $0.31 < a/b < 0.58$. Eq. (6.7) provided a reasonable approximation for $\beta_{p,opt}$, which was found to be invariant with Re_ϕ and C_w. Computations showed that the radial distribution of disc temperature could have a significant effect on the value of $\beta_{p,opt}$. All these parameters are likely to affect the cooling-air temperature, as discussed below.

6.3. Cooling-air temperature

From Eqs. (4.16) and (4.12), the total-temperature difference between the blade-cooling holes and the pre-swirl nozzles is given by

$$T_{t,2} - T_{0,1} = \pi\left(1 - \frac{a^2}{b^2}\right)\frac{Nu_{av}}{PrC_w}(T_s - T_{s,ad})_{av} - \left(2\frac{r_1^2}{r_2^2}\beta_p - 1\right)\frac{\Omega^2 r^2}{2c_p}. \tag{6.8}$$

The first term on the right-hand side of Eq. (6.8) is the heat transfer term; the second is the adiabatic work term.

Consider the case where $T_{0,1}$, Re_ϕ, C_w and the geometric parameters are fixed. The effect of β_p on the work term is monotonic: increasing β_p reduces $T_{t,2}$. The effect of β_p on the heat transfer term is more complicated: it was shown in Section 6.2 that Nu_{av} reaches a minimum when $\beta_p = \beta_{p,opt}$. For $\beta_p < \beta_{p,opt}$, the heat transfer and work terms are in conjunction: $T_{t,2}$ decreases as β_p increases. For $\beta_p > \beta_{p,opt}$, the two terms are in opposition: whether $T_{t,2}$ increases or decreases as β_p increases will depend on the relative magnitude of these terms.

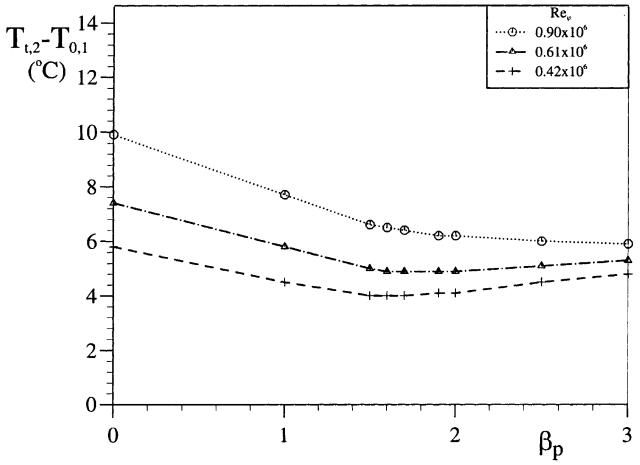

Fig. 12. Computed effect of Re_ϕ on variation of $T_{t,2} - T_{0,1}$ with β_p for $Pr = 0.71$ and $C_w = 1.28 \times 10^4$.

Fig. 12 shows the computed variation of $T_{t,2} - T_{0,1}$ with β_p. The computations were conducted for air with one flow rate, one disc temperature distribution and three values of Re_ϕ. The effects referred to above can be seen: for $Re_\phi = 0.9 \times 10^6$, the work term dominates and $T_{t,2}$ decreases monotonically as β_p increases; for $Re_\phi = 0.61 \times 10^6$ and 0.42×10^6, $T_{t,2}$ decreases with β_p when $\beta_p < \beta_{p,opt}$ and increases when $\beta_p > \beta_{p,opt}$.

Karabay (1998) carried out similar computations for other values of Re_ϕ and C_w and for other distributions of disc temperature. The trends were similar to those discussed here.

7. Conclusions

The flow and heat transfer in a simplified model of a pre-swirl rotating-disc system has been studied theoretically and computationally, and the Reynolds analogy has been used to throw light on this complicated problem. The computational ranges of parameters were: $0.1 < \lambda_T < 0.4$, $0.6 \times 10^6 < Re_\phi < 1.8 \times 10^6$, $5800 < C_w < 23000$, $0 < \beta_p < 6$ and $r_1/r_2 = 0.5$. Although the rotational Reynolds numbers were significantly lower than those in the cooling systems of gas-turbine engines, the resulting flow structures are considered to be representative of those found in many practical cases. The principal conclusions are summarised below:

- Computed values of the adiabatic-disc temperature, $T_{s,ad}$, and the local Nusselt number, Nu, are in good agreement with theoretical relationships derived using the Reynolds analogy.
- It has been shown theoretically that there is a critical pre-swirl ratio, $\beta_{p,crit}$, at which the moment coefficient, C_m, is zero, and there is an optimal pre-swirl ratio, $\beta_{p,opt}$, at which the average Nusselt number, Nu_{av}, is a minimum. Computations have shown that $C_m = 0$ when $\beta_p = \beta_{p,crit}$; they have also confirmed the existence of a minimum value of Nu_{av} when $\beta_p = \beta_{p,opt}$.
- For $\beta_p < \beta_{p,opt}$, the total temperature of the blade-cooling air, $T_{t,2}$, decreases as β_p increases. For $\beta_p > \beta_{p,opt}$, whether $T_{t,2}$ decreases or increases as β_p increases depends on the relative magnitude of the heat transfer and the work terms in the energy equation.

Acknowledgements

The authors thank the Engineering and Physical Sciences Research Council and Alstom Power (UK Ltd) for funding this research project. We also thank the referees for their helpful and constructive comments.

Appendix A. The Reynolds analogy for a rotating cavity

The Reynolds analogy given by Owen and Rogers (1995) can be used to determine the relationships between the shear stress and heat flux, and between the moment coefficient and the average Nusselt number, in the rotating cavity considered in Section 5; it can also be used to determine the adiabatic-disc temperature. For the conditions specified below, the Reynolds analogy is exact for boundary-layer flows; it holds approximately for some elliptic flows. The salient points are given below.

In rotating boundary-layer flows, there is radial outflow in the boundary layer on the disc when $V_{\phi,\infty} < \Omega r$ and radial inflow when $V_{\phi,\infty} > \Omega r$, where $V_{\phi,\infty}$ is the tangential component of velocity in the core outside the boundary layer. The radius, r_* say, where $V_{\phi,\infty} = \Omega r_*$, corresponds to a stagnation point on the disc: for $r > r_*$, the flow in the boundary layer is radially outward; for $r < r_*$, the flow is inward.

The total enthalpy H is defined as

$$H = c_p T + \tfrac{1}{2}(V_r^2 + V_\phi^2) + k' p/\rho, \tag{A.1}$$

where $k' = 0$ for a perfect gas and $k' = 1$ for incompressible flow. H_* is a constant reference enthalpy, chosen as

$$H_* = H(r_*, 0) = c_p T_{s,*} + \tfrac{1}{2}\Omega^2 r_*^2 + k' p/\rho. \tag{A.2}$$

The solutions of the boundary layer momentum and energy equations will be similar for the case where the Prandtl number is unity and

$$\text{(i)} \qquad H_s - H_* = C\Omega^2(r^2 - r_*^2), \tag{A.3}$$

$$\text{(ii)} \qquad \frac{\partial}{\partial z}(H(r,z) - H_*) \to 0 \quad \text{as } z \to \infty, \tag{A.4}$$

$$\text{(iii)} \qquad H(r_*, z) = H_*, \tag{A.5}$$

where C is an arbitrary constant.

Under the above conditions, it can be shown (see Owen and Rogers, 1995) that

$$\frac{H - H_*}{H_s - H_*} = \frac{rV_\phi - \Omega r_*^2}{\Omega(r^2 - r_*^2)}, \tag{A.6}$$

$$\frac{H - H_\infty}{H_s - H_\infty} = \frac{V_\phi - V_{\phi,\infty}}{\Omega r - V_{\phi,\infty}}, \tag{A.7}$$

$$\frac{H - H_s}{H_s - H_\infty} = \frac{V_\phi - \Omega r}{\Omega r - V_{\phi,\infty}} \tag{A.8}$$

and

$$\frac{q_s}{\tau_{\phi,s}} = -c_p \frac{(\partial T/\partial z)_s}{(\partial V_\phi/\partial z)_s}. \tag{A.9}$$

Eq. (A.9) can be evaluated by differentiating Eq. (A.7) to give

$$\frac{q_s}{\tau_{\phi,s}} = -\frac{c_p(T_s - T_\infty) - (1/2)\Omega^2 r^2(1 - (V_{\phi,\infty}/\Omega r))}{\Omega r - V_{\phi,\infty}}. \tag{A.10a}$$

Alternatively, using Eq. (A.6)

$$\frac{q_s}{\tau_{\phi,s}} = -\frac{c_p(T_s - T_{s,*}) - (1/2)\Omega^2 r^2(1 - (r_*^2/r^2))}{\Omega r(1 - (r_*^2/r^2))}. \tag{A.10b}$$

The adiabatic-disc temperature, $T_{s,ad}$, can be found by putting q_s to zero in Eqs. (A.10a) and (A.10b). This gives

$$T_{s,ad} = T_\infty + \frac{\Omega^2 r^2}{2c_p}\left(1 - \frac{V_{\phi,\infty}}{\Omega r}\right)^2 \tag{A.11a}$$

and

$$T_{s,ad} = T_{s,*} + \frac{\Omega^2 r^2}{2c_p}\left(1 - \frac{r_*^2}{r^2}\right). \tag{A.11b}$$

For $Pr = 1$, which is the case considered here, Eqs. (A.11a) and (A.11b) are equivalent. The case when $Pr \neq 1$ is discussed in Section 5.1.

References

Chen, J., Owen, J.M., Wilson, M., 1993a. Parallel-computing techniques applied to rotor-stator systems: fluid dynamics computations. In: Numerical Methods in Laminar and Turbulent Flow, vol. 8. Pineridge, Swansea, pp. 899–911.

Chen, J., Owen, J.M., Wilson, M., 1993b. Parallel-computing techniques applied to rotor-stator systems: thermal computations. In: Numerical Methods in Thermal Problems, vol. 8. Pineridge, Swansea, pp. 1212–1226.

Chew, J.W., Rogers, R.H., 1988. An integral method for the calculation of turbulent forced convection in a rotating cavity with radial outflow. Int. J. Heat Fluid Flow 9, 37–48.

El-Oun, Z., Owen, J.M., 1989. Pre-swirl blade-cooling effectiveness in an adiabatic rotor-stator system. J. Turbomachinery 111, 522–529.

Karabay, H., 1998. Flow and heat transfer in a cover-plate pre-swirl rotating-disc system. Ph.D. thesis, University of Bath, UK.

Karabay, H., Chen, J.X., Pilbrow, R., Wilson, M., Owen, J.M., 1999. Flow in a cover-plate pre-swirl rotor-stator system. J. Turbomachinery 121, 160–166.

Karabay, H., Pilbrow, R., Wilson, M., Owen, J.M., 2000. Performance of pre-swirl rotating-disc systems. J. Eng. Gas Turbines Power 122, 442–450.

Launder, B.E., Sharma, B.I., 1974. Application of the energy dissipation model of turbulence to the calculation of the flow near a spinning disc. Lett. Heat Mass Transfer 1, 131–138.

Meierhofer, B., Franklin, C.J., 1981. An investigation of a pre-swirled cooling airflow to a gas turbine disk by measuring the air temperature in the rotating channels. ASME Paper 81-GT-132.

Morse, A.P., 1988. Numerical prediction of turbulent flow in rotating cavities. J. Turbomachinery 110, 202–215.

Morse, A.P., 1991. Assessment of laminar-turbulent transition in closed disc geometries. J. Turbomachinery 113, 131–138.

Owen, J.M., 1971. The Reynolds analogy applied to flow between a rotating and a stationary disc. Int. J. Heat Mass Transfer 14, 451–460.

Owen, J.M., Rogers, R.H. 1989. Flow and heat transfer in rotating disc systems. Rotor-stator Systems, vol. 1. Research Studies Press, Taunton, UK/Wiley, New York.

Owen, J.M., Rogers, R.H. 1995. Flow and heat transfer in rotating disc systems. In: Rotating Cavities, vol. 2. Research Studies Press, Taunton, UK/Wiley, New York.

Pilbrow, R., Karabay, H., Wilson, M., Owen, J.M., 1999. Heat transfer in a cover-plate pre-swirl rotating-disc system. J. Turbomachinery 121, 249–256.

Popp, O., Zimmermann, H., Kutz, J. 1996. CFD analysis of cover-plate receiver flow. ASME Paper 96-GT-357.

Wilson, M., Pilbrow, R., Owen, J.M., 1997. Flow and heat transfer in a pre-swirl rotor-stator system. J. Turbomachinery 119, 364–373.